

Article

Bandgap Engineering of Two-Dimensional Double Perovskite Cs₄AgBiBr₈/WSe₂ Heterostructure from Indirect Bandgap to Direct Bandgap by Introducing Se Vacancy

Yiwei Cai ¹, Zhengli Lu ², Xin Xu ², Yujia Gao ², Tingting Shi ^{2,3,*} , Xin Wang ^{1,4,*}  and Lingling Shui ^{1,5}

¹ School of Information and Optoelectronic Science and Engineering, South China Normal University, Guangzhou 510006, China; shuill@m.scnu.edu.cn (L.S.)

² Siyuan Laboratory, Department of Physics, Jinan University, Guangzhou 510632, China

³ Guangzhou Key Laboratory of Vacuum Coating Technologies and New Energy Materials, Jinan University, Guangzhou 510632, China

⁴ International Academy of Optoelectronics at Zhaoqing, South China Normal University, Guangzhou 510006, China

⁵ Guangdong Provincial Key Laboratory of Nanophotonic Functional Materials and Device, South China Normal University, Guangzhou 510006, China

* Correspondence: ttshi@jnu.edu.cn (T.S.); wangxin@scnu.edu.cn (X.W.)

Abstract: Heterostructures based on layered materials are considered next-generation photocatalysts due to their unique mechanical, physical, and chemical properties. In this work, we conducted a systematic first-principles study on the structure, stability, and electronic properties of a 2D monolayer WSe₂/Cs₄AgBiBr₈ heterostructure. We found that the heterostructure is not only a type-II heterostructure with a high optical absorption coefficient, but also shows better optoelectronic properties, changing from an indirect bandgap semiconductor (about 1.70 eV) to a direct bandgap semiconductor (about 1.23 eV) by introducing an appropriate Se vacancy. Moreover, we investigated the stability of the heterostructure with Se atomic vacancy in different positions and found that the heterostructure was more stable when the Se vacancy is near the vertical direction of the upper Br atoms from the 2D double perovskite layer. The insightful understanding of WSe₂/Cs₄AgBiBr₈ heterostructure and the defect engineering will offer useful strategies to design superior layered photodetectors.

Keywords: van der Waals heterostructure; first-principles; electronic properties; bandgap engineering



Citation: Cai, Y.; Lu, Z.; Xu, X.; Gao, Y.; Shi, T.; Wang, X.; Shui, L. Bandgap Engineering of Two-Dimensional Double Perovskite Cs₄AgBiBr₈/WSe₂ Heterostructure from Indirect Bandgap to Direct Bandgap by Introducing Se Vacancy. *Materials* **2023**, *16*, 3668. <https://doi.org/10.3390/ma16103668>

Academic Editor: Sergey Kukushkin

Received: 16 March 2023

Revised: 28 April 2023

Accepted: 5 May 2023

Published: 11 May 2023



Copyright: © 2023 by the authors. Licensee MDPI, Basel, Switzerland. This article is an open access article distributed under the terms and conditions of the Creative Commons Attribution (CC BY) license (<https://creativecommons.org/licenses/by/4.0/>).

1. Introduction

Organic–inorganic metal halide perovskites demonstrate high performance, but still face one major challenge: a stability issue due to hydrophilic organic cations and displaying very low thermal decomposition temperatures. Recently, all-inorganic halide perovskites, especially the double perovskite, without molecules and lead-free perovskite showing excellent stability against moisture, heat, and light, have attracted extensive attention [1–3]. In general, since the 2D all-inorganic double perovskite Cs₄AgBiBr₈ has a high exciton-binding energy, which is 3 times larger than that of the 3D all-inorganic double perovskite Cs₂AgBiBr₆, the charge carrier mobility and absorption coefficients of Cs₄AgBiBr₈ (2D) in the visible spectrum are worse than those of Cs₂AgBiBr₆ (3D) [4]. However, in 2021, Wang et al. reported the upconversion photovoltaic effect of WS₂ monolayer/(C₆H₅C₂H₄NH₃)₂PbI₄ 2D perovskite heterostructures by below-bandgap two-photon absorption via a virtual intermediate state, which enables heterojunction devices with good photoresponsivity and excellent current on/off ratio [5]. Therefore, heterostructure is considered an efficient way to enhance device performance, especially the charge mobility and light adsorption.

Furthermore, van der Waals heterostructures (vdWHs) based on 2DLMs (2D layered materials) with selectable material properties pave the way to build new structures at the

atomic scale, which may lead to new heterostructures with novel physical properties and versatility [6,7]. Two-dimensional layered materials, such as graphene and transition metal dichalcogenides (TMDs), have attracted great attention due to their extraordinary properties in fundamental physics and potential applications [8,9]. Interestingly, MoX_2 and WX_2 ($X = \text{S}, \text{Se}, \text{Te}$) TMDs are indirect gap semiconductors in their bulk states, but some of them can become direct gap semiconductors when the film thickness is intentionally changed into a monolayer [10–12]. Due to the weakened dielectric shielding and layer-dependent electronic structure, monolayer TMDs such as MoS_2 and WSe_2 have direct band gaps with strong exciton characteristics in the visible or near-infrared range [13]. However, their relatively weak light absorption hinders their practical application. Fang et al. reported that integrating monolayer TMDs with 2D perovskites, which serve as the light-absorption layer, can be an efficient solution. Through the complementary effect of two-dimensional perovskites, heterostructure engineering based on TMD layers can effectively improve the performance of photodetectors with low-power optoelectronic applications [14].

A TMD, WSe_2 , has recently received more attention [15–17]. Two-dimensional WSe_2 thin films and Nanoflakes have been used for photoelectrochemical hydrogen production [18,19]. In this work, we used first-principles calculations to investigate the effect of WSe_2 layer defects on the heterostructure properties of a monolayer WSe_2 /monolayer $\text{Cs}_4\text{AgBiBr}_8$ heterostructure. Our computational results show that the heterostructure exhibits an indirect band gap where the CBM (conduction band minimum) and VBM (valence band maximum) positions locate at different k points when the WSe_2 monolayer is combined with the $\text{Cs}_4\text{AgBiBr}_8$ monolayer. Xia et al. reported that when the atom vacancy defect of vdWHs generates a flat defect energy level [20], we can employ the strategy of defect modification and successfully change the heterostructure from an indirect band gap to a direct band gap by introducing the defect energy level. Finally, the obtained heterostructure with a Se vacancy exhibits a direct band gap, and the heterostructure is more stable when the Se vacancy is near the vertical direction of the upper Br atoms from the 2D double perovskite layer.

2. Calculation Methods

Our first-principles calculations were performed using density functional theory (DFT) [21,22], which is implemented in the VASP code [23,24] with the standard frozen-core projector-augmented wave (PAW) [25] method. We used the generalized gradient approximation (GGA) [26] by the Perdew–Burke–Ernzerhof (PBE) method [27] to relax the structure. The cut-off energy is set to 400 eV. We used a $2 \times 3 \times 1$ k -points Γ -centered mesh for calculating total energy and the structure relaxations of the $\text{WSe}_2/\text{Cs}_4\text{AgBiBr}_8$ heterostructure, $\text{WSe}_2/\text{Cs}_4\text{AgBiBr}_8$ heterostructure with W vacancy, and $\text{WSe}_2/\text{Cs}_4\text{AgBiBr}_8$ heterostructure with Se vacancy. A Γ -centered mesh of $9 \times 9 \times 2$ k -points was used for the calculations of the WSe_2 monolayer. All structures were relaxed until the energy was less than 10^{-5} eV per atom and the force on each ion reduced below $0.03 \text{ eV } \text{\AA}^{-1}$. Then the electronic properties were calculated with the optimized structures. Considering the underestimation of the GGA–PBE functional of the band gaps, we employed the Heyd–Scuseria–Ernzerhof (HSE06) hybrid functional [28] to calculate the electronic structure of the WSe_2 monolayer and $\text{Cs}_4\text{AgBiBr}_6$ monolayer for accurate band gap value.

3. Results and Discussion

3.1. Construction and Stability of the Heterostructure

We first investigated the structure of the WSe_2 monolayer and $\text{Cs}_4\text{AgBiBr}_8$. The WSe_2 monolayer is built by the monolayer 2D structure separated from WSe_2 bulk (space group: $P6_3mmc$ and lattice parameters: $a = 3.327 \text{ \AA}$, $c = 15.069 \text{ \AA}$ from [29,30]) and adding a vacuum layer of 15 \AA . We analyzed the WSe_2 monolayer using the GGA–PBE method; the space group is $P\bar{6}m2$, and the optimized lattice parameters are $a = 3.315 \text{ \AA}$ and $c = 18.031 \text{ \AA}$. We constructed a single-layer two-dimensional double perovskite $\text{Cs}_4\text{AgBiBr}_8$ by cutting the

(0 1 1) surface of the double perovskite $\text{Cs}_2\text{AgBiBr}_6$ (space group: $Fm\bar{3}m$; lattice parameters: $a = 8.123 \text{ \AA}$). To ensure that the analysis object is the $\text{Cs}_4\text{AgBiBr}_8$ monolayer, we added a vacuum layer of 15 \AA [31] to the unit cell of $\text{Cs}_4\text{AgBiBr}_8$ to avoid the effect of periodicity. We analyzed the WSe_2 monolayer with the GGA–PBE method; the space group is $P4mmm$, and the optimized lattice parameters are $a = 8.123 \text{ \AA}$ $c = 20.782 \text{ \AA}$.

Heterostructures were built by the Structural Utilities (804) of ‘vaspkit’ [32] to find two representative heterostructures containing 73 atoms (containing 8 Cs, 2 Ag, 2 Bi, 16 Br, 15 W, and 30 Se atoms) with a suitable lattice shape and reasonable lattice mismatch respectively, named Heterostructure A and Heterostructure B (shown in Figure 1). The lattice mismatch rate σ (the lattice mismatch which can quantify structural match of crystals) is 2.027% and 4.048%, respectively, less than 5%. Heterostructure A is obtained by expanding the

WSe_2 single crystal according to the transformation matrix $\begin{bmatrix} 0 & 5 & 0 \\ 3 & 4 & 0 \\ 0 & 0 & 1 \end{bmatrix}$, and the supercell

is obtained by the $\text{Cs}_4\text{AgBiBr}_8$ single crystal expanding according to the transformation matrix $\begin{bmatrix} 0 & 2 & 0 \\ 1 & 1 & 0 \\ 0 & 0 & 1 \end{bmatrix}$. Heterostructure B is obtained by expanding the WSe_2 single crystal

according to the transformation matrix $\begin{bmatrix} 1 & 4 & 0 \\ 5 & 5 & 0 \\ 0 & 0 & 1 \end{bmatrix}$, and the supercell is obtained by the

$\text{Cs}_4\text{AgBiBr}_8$ single crystal expanding according to the transformation matrix $\begin{bmatrix} 1 & 1 & 0 \\ 0 & 2 & 0 \\ 0 & 0 & 1 \end{bmatrix}$.

Following several attempts, the vacuum layer of the two species in the heterostructure is set to 3.5 \AA . In order to avoid the influence of periodicity on the calculation results, a vacuum layer of 15 \AA is set outside the heterostructure.

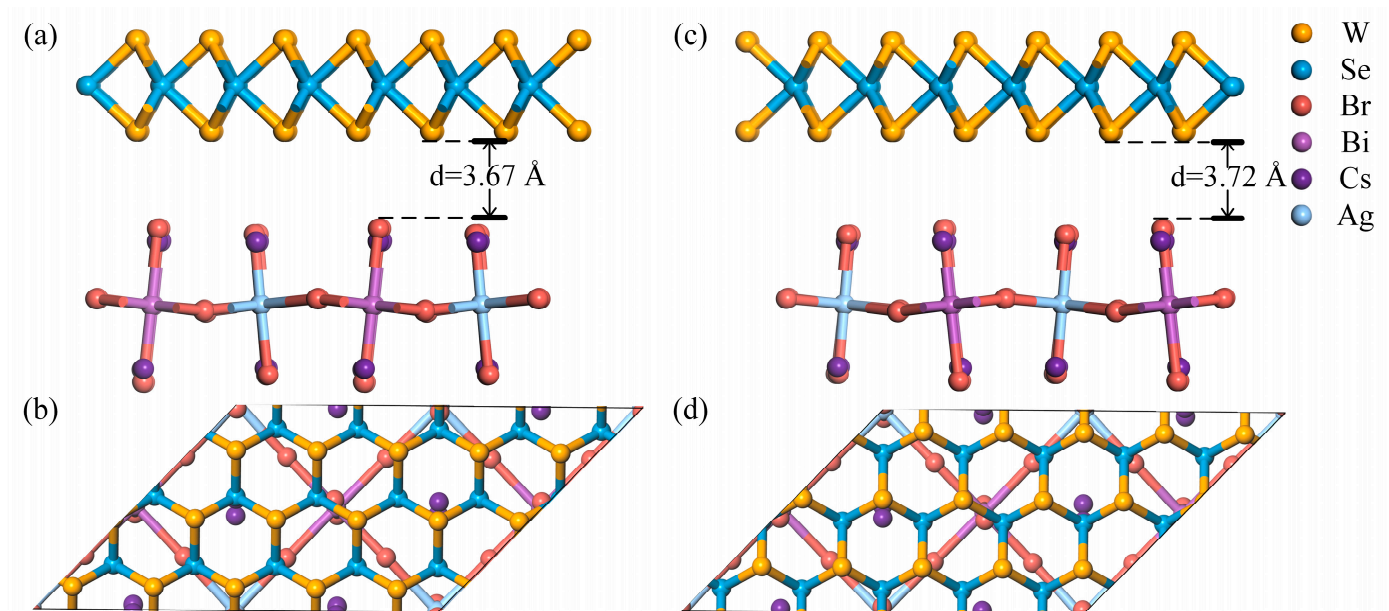


Figure 1. (a) Side and (b) top views of Heterostructure A; (c) side and (d) top views of Heterostructure B.

The two types of heterostructure are very similar; Heterostructure B can be obtained from Heterostructure A when the W atom and the vertical two Se atoms are exchanged in the horizontal direction. Interestingly, in the vertical direction, the atoms position correspondences are different; the calculated results show that the properties of the two heterostructures are basically the same. In order to quantify the thermodynamic stability of

the interaction between WSe_2 and $Cs_4AgBiBr_8$, the interface adhesion energy E_{ad} , a good descriptor, is obtained according to Equation (1):

$$E_{ad} = E_{hete.} - E_{WSe_2} - E_{Cs_4AgBiBr_8}, \quad (1)$$

where $E_{hete.}$, E_{WSe_2} , and $E_{Cs_4AgBiBr_8}$ represent the total energies of the relaxed heterostructures $WSe_2/Cs_4AgBiBr_8$, monolayer WSe_2 , and monolayer $Cs_4AgBiBr_8$, respectively. We calculated the adhesion energy of the two heterostructures to be -0.226 eV and -0.219 eV, respectively. Obviously, Heterostructure A has lower adhesion energy and lattice mismatch rate, so we decided to use Heterostructure A for follow-up research.

After geometric optimization, the surface of WSe_2 did not exhibit significant deformation. The $WSe_2/Cs_4AgBiBr_8$ heterostructure has a typical vdW equilibrium spacing, which was calculated to be 3.67 Å (Figure 1a) between the WSe_2 and $Cs_4AgBiBr_8$ layers. We noticed that when WSe_2 was adsorbed onto the surface of $Cs_4AgBiBr_8(001)$, only physical adsorption occurred, but no chemical adsorption was observed.

3.2. Electronic Properties of $WSe_2/Cs_4AgBiBr_8$

To investigate the photocatalytic performance of the $WSe_2/Cs_4AgBiBr_8$ heterostructure, the energy band structures of the WSe_2 monolayer, $Cs_4AgBiBr_8$ monolayer, and $WSe_2/Cs_4AgBiBr_8$ heterostructure were calculated, respectively. We employed GGA–PBE and HSE06 methods to acquire more exact electronic structure properties, as shown in Figure 2. The WSe_2 monolayer has a direct bandgap of 1.55 eV with the GGA–PBE method, which agrees well with the 1.6 eV estimated by extrapolating, as shown in Figure 2a. For the WSe_2 monolayer, CBM and VBM are located at the K point, while the $Cs_4AgBiBr_8$ monolayer has an indirect bandgap of 2.09 eV, as shown in Figure 2b. With the HSE06 method, the WSe_2 monolayer has a direct bandgap of 2.03 eV, and the bandgap of $Cs_4AgBiBr_8$ monolayer is 3.23 eV. Thus, the GGA–PBE functional might underestimate the band gaps of the heterostructures that we built, by about 0.6 eV, at least.

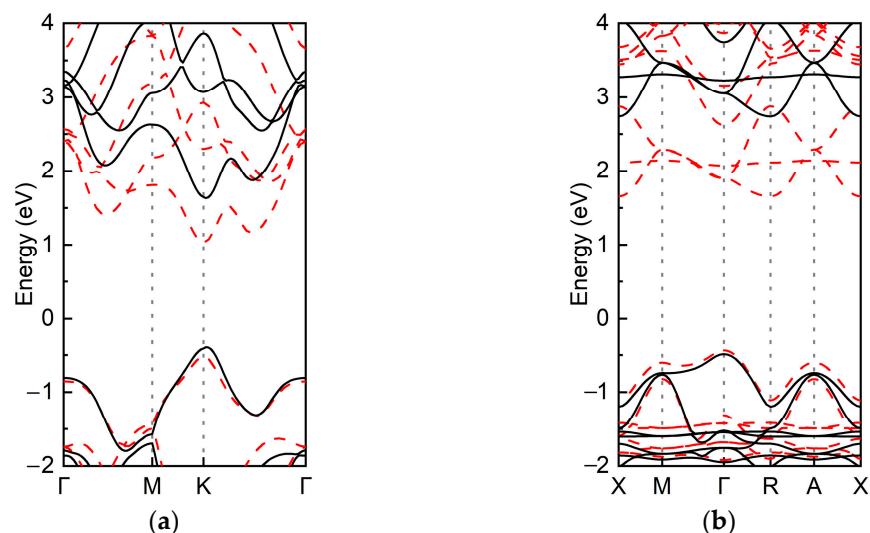


Figure 2. Energy band structures of the (a) WSe_2 monolayer and (b) $Cs_4AgBiBr_8$ monolayer with PBE (red dashed lines) and HSE (black solid lines) methods.

The $WSe_2/Cs_4AgBiBr_8$ heterostructure is a type-II heterostructure which has better photocatalytic performance, owing to its effectiveness in spatially separating photogenerated electron-hole pairs by band alignment between two semiconductors [33]. By comparing the band structures of the $Cs_4AgBiBr_8$ monolayer and the WSe_2 monolayer, we found that the band structure of the $WSe_2/Cs_4AgBiBr_8$ heterostructure is influenced by vdW interaction between $Cs_4AgBiBr_8$ and WSe_2 interfaces, rather than an uncomplicated superposition of the WSe_2 monolayer and the $Cs_4AgBiBr_8$ monolayer. The energy bands of

$\text{WSe}_2/\text{Cs}_4\text{AgBiBr}_8$ heterostructures are staggered around the forbidden band, as shown in Figure 3a, in which the red and blue parts are contributed by $\text{Cs}_4\text{AgBiBr}_8$ and WSe_2 , respectively. The band structure of the $\text{WSe}_2/\text{Cs}_4\text{AgBiBr}_8$ heterostructure has an indirect bandgap of 1.10 eV using the GGA–PBE method, which did not meet our expectations. The VBM and CBM of the heterostructure were located at Γ point and the point between the Γ point and X point, respectively. Obviously, the $\text{Cs}_4\text{AgBiBr}_8$ monolayer contributes the VBM, and the CBM comes from the WSe_2 monolayer. Learning from the total and atom-projected density of states (TDOS and PDOS) between -1.5 eV and 1.5 eV, as shown in Figure 3a, the VBM is mainly composed of Ag d state and Br p state; at the same time, the CBM is mainly composed of W d state and Se p state.

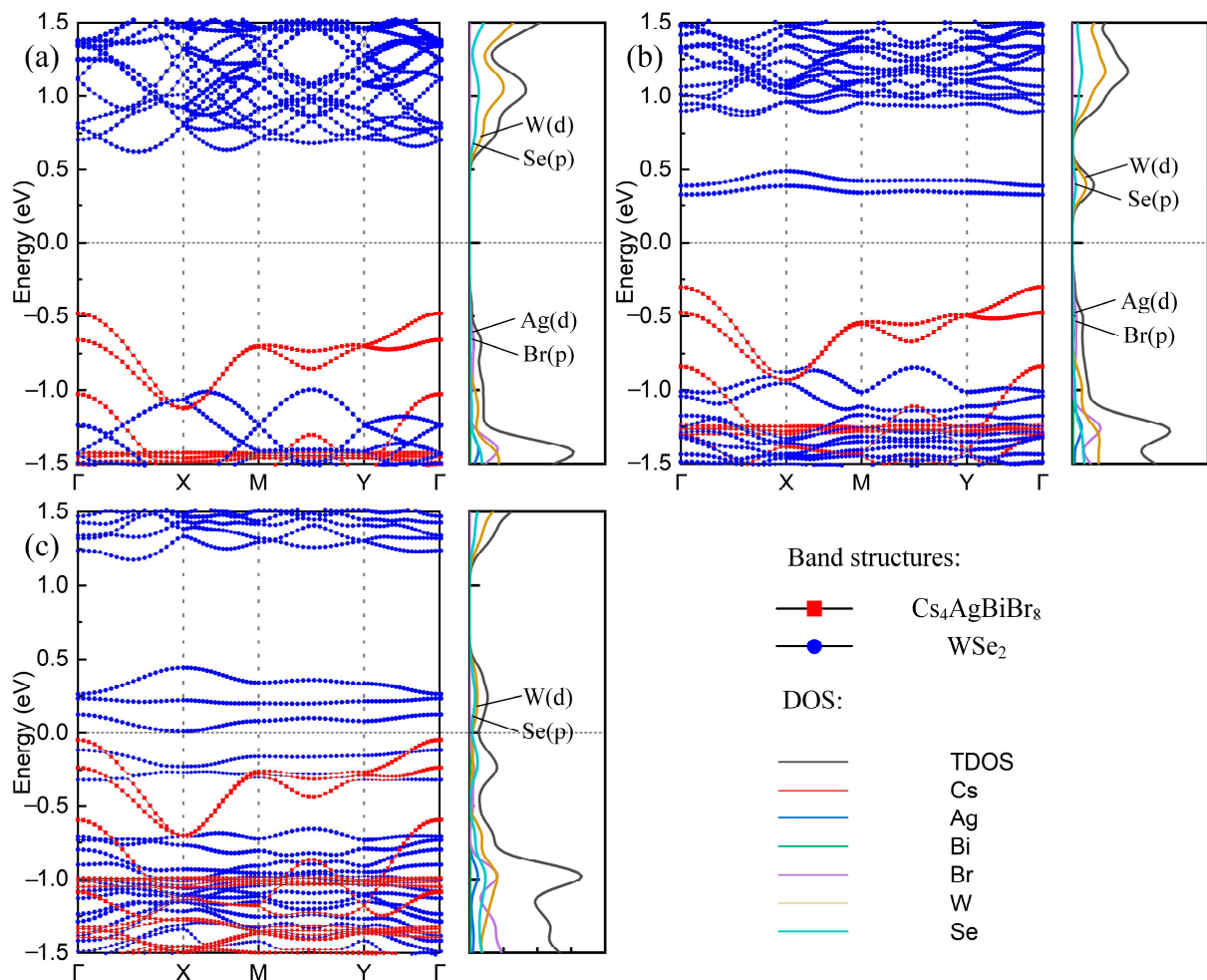


Figure 3. The projected band structures (left) and the DOS (right) of the (a) $\text{Cs}_4\text{AgBiBr}_8/\text{WSe}_2$ heterostructure, (b) $\text{Cs}_4\text{AgBiBr}_8/\text{WSe}_2$ heterostructure with No. 6 Se vacancy, and (c) $\text{Cs}_4\text{AgBiBr}_8/\text{WSe}_2$ heterostructure with W vacancy. The red square and blue circle in the band structures show the electron orbits of $\text{Cs}_4\text{AgBiBr}_8$ and WSe_2 , respectively.

The VBM of $\text{WSe}_2/\text{Cs}_4\text{AgBiBr}_8$ heterostructure is provided by the $\text{Cs}_4\text{AgBiBr}_8$ layer, while the CBM is provided by the WSe_2 layer. This demonstrates that the holes and excited electrons are separately confined to different layers of the heterostructure, which promotes the formation of spatially indirect excitons.

3.3. $\text{Cs}_4\text{AgBiBr}_8/\text{WSe}_2$ with Defects

3.3.1. $\text{Cs}_4\text{AgBiBr}_8/\text{WSe}_2$ with W Vacancy

It can be learned from Figure 3c that W atoms play a major role in the CBM, so the effect of adding W vacancies to the heterostructure is also considered. The WSe_2 layer consists of 15 WSe_2 molecules with a total of 15 W atoms and 30 Se atoms. We attempted to analyze 15 different heterostructures with W atom vacancies using the GGA–PBE method (one of which is shown in Figure S1a). Electronic properties of 15 W atom vacancy heterostructures are similar and not ideal. It can be learned from the energy band structures and the DOS (Figure 3c) that the defect states brought by the W vacancies are generated near the VBM and coincide with the VBM, which makes both sides of the forbidden band provided by WSe_2 and the band gap is still indirect, which is not conducive to improving the photocatalytic activity.

3.3.2. Stability of $\text{Cs}_4\text{AgBiBr}_8/\text{WSe}_2$ with Se Vacancy

$\text{WSe}_2/\text{Cs}_4\text{AgBiBr}_8$ heterostructure is an indirect band gap heterostructure, which is not conducive to improving the photocatalytic activity, and the positions of VBM and CBM are very close, so we tried to introduce defects in the heterostructure. The VBM provided by $\text{Cs}_4\text{AgBiBr}_8$ is located at the Γ point, while the CBM provided by WSe_2 is located between the Γ point and the X point, not on the ordinary high symmetry point. Compared with the 2D double perovskite $\text{Cs}_4\text{AgBiBr}_8$ layer, the WSe_2 layer has better ductility. Combining the above two points, we decided to study the WSe_2 layers in $\text{WSe}_2/\text{Cs}_4\text{AgBiBr}_8$, namely the W vacancy and the Se vacancy defects.

Interestingly, we found that the introduction of Se atomic vacancy evidently affects the electronic properties of the heterostructures. We numbered the 30 Se atoms in the WSe_2 layer as 1 to 30 (as shown in Figure 4a), where the odd numbers are the upper layer, and the even numbers are the lower layer. The calculated results show that all 30 $\text{Cs}_4\text{AgBiBr}_8/\text{WSe}_2$ heterostructures with Se atom vacancies are very close in electronic properties and all have direct band gaps, two of which are shown in Figure S2. Compared to the original heterostructure, that with Se atom vacancies shows minimal structure change. We therefore calculated the adhesion energies of 30 heterostructures with Se atom vacancy (Figure 4b). We found that the adhesion energy of most of the 30 heterostructures with Se atom vacancy is around -0.225 eV, and the heterostructures have lower interfacial adhesion energy when the defects appear on the lower surface of the WSe_2 layer. Clearly, we observe that the heterostructures with No. 6 Se vacancy and the No. 14 Se vacancy have abnormally low adhesion energies. Both of the heterostructures with No. 6 Se vacancy and No. 14 Se vacancy are near the vertical direction of the upper Br atoms from the 2D double perovskite layer. The abnormally low interfacial adhesion energy may be caused by this Br atom.

3.3.3. Electronic Structure of $\text{Cs}_4\text{AgBiBr}_8/\text{WSe}_2$ with Se Vacancy

We analyzed $\text{Cs}_4\text{AgBiBr}_8/\text{WSe}_2$ heterostructures with No. 6 Se vacancy (shown in Figure S1b), which has the lowest adhesion energy. We found a defect level provided by WSe_2 between the Fermi level and the conduction band, which is quite flat and reaches a minimum at the Γ point (Figure 3b). Compared with the $\text{Cs}_4\text{AgBiBr}_8/\text{WSe}_2$ heterostructure energy band structure (Figure 3a), the Se atom vacancy has little effect on the valence band, and the VBM is still located at the Γ point. Therefore, we speculate that the $\text{Cs}_4\text{AgBiBr}_8/\text{WSe}_2$ heterostructure with Se atom vacancy has a direct band gap of 0.63 eV, and both VBM and CBM are located at the Γ point.

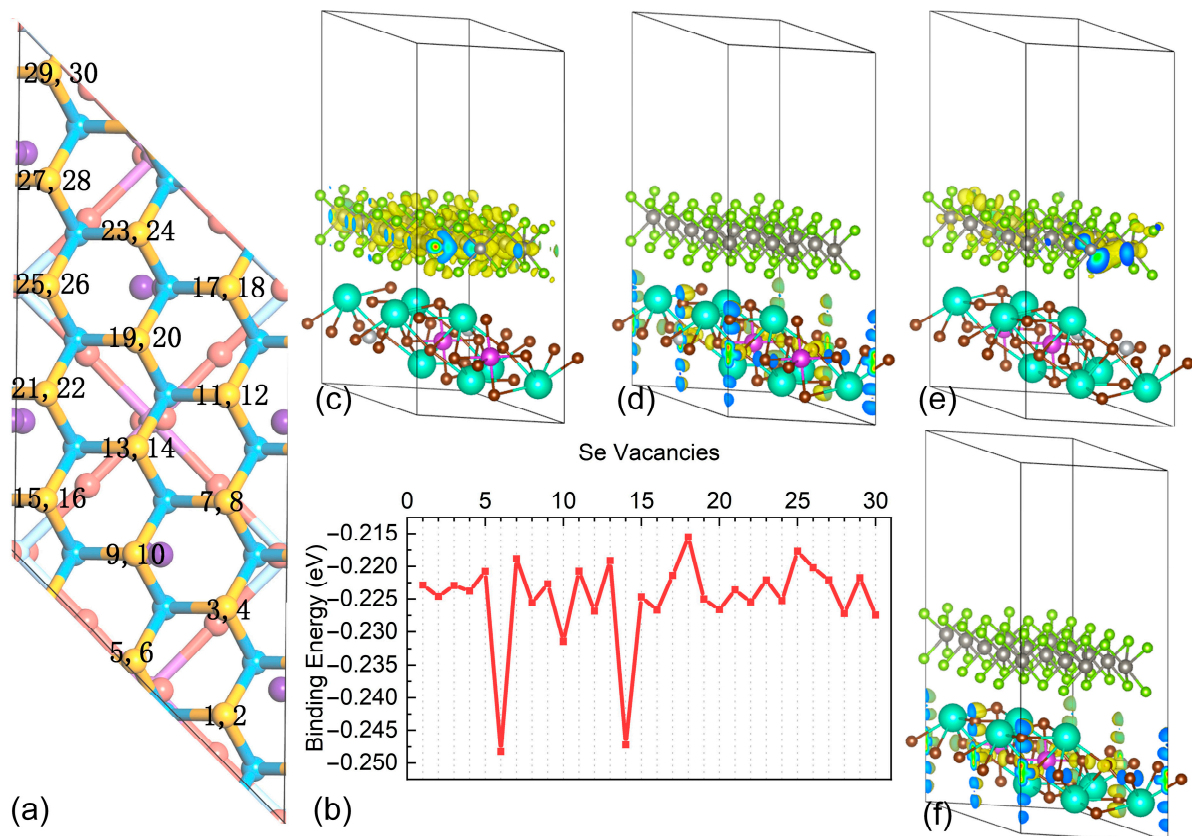


Figure 4. (a) Se atoms ($n = 30$) in the WSe₂ layer of the heterostructure with Se atom vacancy defects. The atoms are numbered 1 to 30, where the odd numbers are the upper layer, and the even numbers are the lower layer. (b) The adhesion energy of Cs₄AgBiBr₈/WSe₂ heterostructures with 30 Se atom vacancy defects (data are shown in Table S1). The partial charge densities of the (c) CBM and (d) VBM of the Cs₄AgBiBr₈/WSe₂ heterostructure, and that of the (e) CBM and (f) VBM of the Cs₄AgBiBr₈/WSe₂ heterostructure with Se vacancy.

We calculated the partial charge densities for the CBM and VBM of the Cs₄AgBiBr₈/WSe₂ heterostructure and of the heterostructure with Se vacancy (shown in Figure 4c–f, respectively). The electron orbitals of WSe₂ and Cs₄AgBiBr₈ occupy the CBM and VBM of the Cs₄AgBiBr₈/WSe₂ heterostructure, respectively, which is consistent with the earlier analysis about DOS. Comparing the partial charge densities of CBM between the original heterostructure and heterostructure with Se vacancy, it is evident that the charge centers on the Se vacancy, which is uniformly distributed in the original heterostructure. The partial charge density of VBM has no change when there is a Se vacancy in the Cs₄AgBiBr₈/WSe₂ heterostructure.

To understand how charges are transferring at the interface, we calculated the work function, which is used as an intrinsic reference for band alignment, of the Cs₄AgBiBr₈ monolayer, WSe₂ monolayer with Se vacancy, and Cs₄AgBiBr₈/WSe₂ with Se vacancy using the GGA–PBE method. The work function is calculated according to Equation (2) [34]:

$$\Phi = E_{vac} - E_{fermi}, \quad (2)$$

where Φ , E_{vac} , and E_{fermi} represent the work function, the electrostatic potential of the vacuum level, and the Fermi level, respectively. Based on Equation (2), the work functions of the Cs₄AgBiBr₈ monolayer, WSe₂ monolayer with Se vacancy, and Cs₄AgBiBr₈/WSe₂ with Se vacancy are 4.33 eV, 5.07 eV, and 4.43 eV, respectively, as shown in Figure 5a–c.

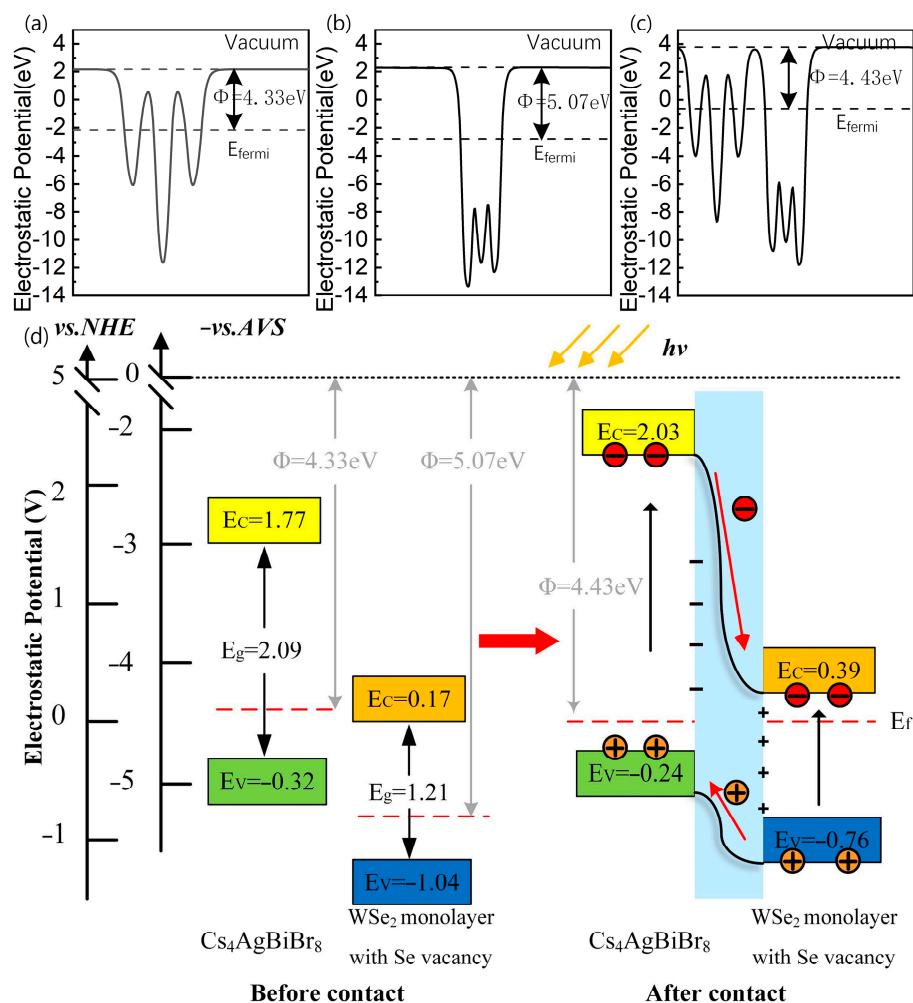


Figure 5. The electrostatic potentials of the (a) $\text{Cs}_4\text{AgBiBr}_8$ monolayer, (b) WSe_2 monolayer with Se vacancy, and (c) $\text{Cs}_4\text{AgBiBr}_8/\text{WSe}_2$ heterostructure with Se vacancy, respectively. (d) The band diagram of the $\text{WSe}_2/\text{Cs}_4\text{AgBiBr}_8$ heterostructure and schematic of the charge separation at its interface under sunlight irradiation.

It can be seen from the electrostatic potentials that the electrons in the $\text{Cs}_4\text{AgBiBr}_8$ layer with low work function flow into the WSe_2 layer, which has high work function after the electrostatic potential contact is formed. Therefore, the negative charges will accumulate at the interface of the WSe_2 layer; at the same time, the positive charges will accumulate at the interface of the $\text{Cs}_4\text{AgBiBr}_8$ layer. Finally, the two Fermi levels of WSe_2 and $\text{Cs}_4\text{AgBiBr}_8$ reach the same energy level; then, an internal electric field, which is generated by this spontaneous interfacial charge transfer, takes shape at the interface from the WSe_2 layer to the $\text{Cs}_4\text{AgBiBr}_8$ layer. We plotted the energy level lineup diagrams and the charge separation schematic of the $\text{Cs}_4\text{AgBiBr}_8$ monolayer and WSe_2 monolayer before and after contact, as shown in Figure 5d.

4. Conclusions

We constructed van der Waals heterostructures using monolayer WSe_2 and monolayer 2D $\text{Cs}_4\text{AgBiBr}_8$. Considering a reasonable lattice mismatch rate and interface adhesion energy, we constructed a new $\text{WSe}_2/\text{Cs}_4\text{AgBiBr}_8$ heterostructure with a lattice mismatch rate of 2.027% and the lowest interface adhesion energy. Importantly, layered $\text{WSe}_2/\text{Cs}_4\text{AgBiBr}_8$ can form a type-II heterostructure. By introducing Se vacancy, we further successfully converted it into a direct band gap $\text{WSe}_2/\text{Cs}_4\text{AgBiBr}_8$ heterostructure. We also found the most stable $\text{WSe}_2/\text{Cs}_4\text{AgBiBr}_8$ heterostructure with Se vacancy, when Se vacancy appeared

on the lower surface of WSe₂ and near the vertical direction of the upper Br atoms from the 2D double perovskite layer. These results indicate that it is possible to construct type-II van-der-Waals heterostructures composed of TMD monolayers and 2D double perovskites from indirect band gaps to direct band gaps based on bandgap engineering.

Supplementary Materials: The following supporting information can be downloaded at: <https://www.mdpi.com/article/10.3390/ma16103668/s1>, Figure S1: the top and side views of Cs₄AgBiBr₈/WSe₂ heterostructure with (a) Se vacancy and (b) W vacancy; Figure S2: the band structures (left) and the DOS (right) of the Cs₄AgBiBr₈/WSe₂ heterostructure with (a) No. 2 Se vacancy and (b) No. 3 Se vacancy; Table S1: The adhesion energy (eV) of 30 Cs₄AgBiBr₈/WSe₂ heterostructures with different Se atom vacancy defects.

Author Contributions: Conceptualization, Y.C. and T.S.; methodology, Y.C. and Y.G.; Validation, Z.L. and X.X.; investigation, Y.C.; resources, X.W. and T.S.; data curation, Z.L. and X.X.; writing—original draft preparation, Y.C.; writing—review and editing, T.S.; visualization, Y.C. and Y.G.; supervision, T.S. and L.S.; Project administration, L.S.; funding acquisition, X.W. All authors have read and agreed to the published version of the manuscript.

Funding: This research was funded by the Outstanding Youth Project of Guangdong Natural Science Foundation, grant number 2021B1515020051.

Institutional Review Board Statement: Not applicable.

Informed Consent Statement: Not applicable.

Data Availability Statement: The data that support the findings of this study are available from the corresponding author upon reasonable request.

Conflicts of Interest: The authors declare no conflict of interest.

References

1. Yang, Y.; You, J. Make Perovskite Solar Cells Stable. *Nature* **2017**, *544*, 155–156. [[CrossRef](#)] [[PubMed](#)]
2. Lei, L.-Z.; Shi, Z.-F.; Li, Y.; Ma, Z.-Z.; Zhang, F.; Xu, T.-T.; Tian, Y.-T.; Wu, D.; Li, X.-J.; Du, G.-T. High-Efficiency and Air-Stable Photodetectors Based on Lead-Free Double Perovskite Cs₂AgBiBr₆ Thin Films. *J. Mater. Chem. C* **2018**, *6*, 7982–7988. [[CrossRef](#)]
3. Slavney, A.H.; Hu, T.; Lindenberg, A.M.; Karunadasa, H.I. A Bismuth-Halide Double Perovskite with Long Carrier Recombination Lifetime for Photovoltaic Applications. *J. Am. Chem. Soc.* **2016**, *138*, 2138–2141. [[CrossRef](#)] [[PubMed](#)]
4. Chen, Y.-L.; Yan, D.-N.; Zeng, M.-W.; Liao, C.-S.; Cai, M.-Q. 2D and 3D Double Perovskite with Dimensionality-Dependent Optoelectronic Properties: First-Principle Study on Cs₂AgBiBr₆ and Cs₄AgBiBr₈. *J. Phys. Condens. Matter* **2021**, *34*, 065501. [[CrossRef](#)]
5. Wang, Q.; Wee, A.T.S. Upconversion Photovoltaic Effect of WS₂/2D Perovskite Heterostructures by Two-Photon Absorption. *ACS Nano* **2021**, *15*, 10437–10443. [[CrossRef](#)]
6. Geim, A.K.; Grigorieva, I.V. Van Der Waals Heterostructures. *Nature* **2013**, *499*, 419–425. [[CrossRef](#)]
7. Zhou, X.; Hu, X.; Yu, J.; Liu, S.; Shu, Z.; Zhang, Q.; Li, H.; Ma, Y.; Xu, H.; Zhai, T. 2D Layered Material-Based van Der Waals Heterostructures for Optoelectronics. *Adv. Funct. Mater.* **2018**, *28*, 1706587. [[CrossRef](#)]
8. Yu, Q.; Luo, Y.; Mahmood, A.; Liu, B.; Cheng, H.-M. Engineering Two-Dimensional Materials and Their Heterostructures as High-Performance Electrocatalysts. *Electrochem. Energy Rev.* **2019**, *2*, 373–394. [[CrossRef](#)]
9. Radisavljevic, B.; Radenovic, A.; Brivio, J.; Giacometti, V.; Kis, A. Single-Layer MoS₂ Transistors. *Nat. Nanotechnol.* **2011**, *6*, 147–150. [[CrossRef](#)]
10. Cong, C.; Shang, J.; Wang, Y.; Yu, T. Optical Properties of 2D Semiconductor WS₂. *Adv. Opt. Mater.* **2018**, *6*, 1700767. [[CrossRef](#)]
11. Ramakrishna Matte, H.S.S.; Gomathi, A.; Manna, A.K.; Late, D.J.; Datta, R.; Pati, S.K.; Rao, C.N.R. MoS₂ and WS₂ Analogues of Graphene. *Angew. Chem. Int. Ed.* **2010**, *49*, 4059–4062. [[CrossRef](#)]
12. Ramasubramaniam, A. Large Excitonic Effects in Monolayers of Molybdenum and Tungsten Dichalcogenides. *Phys. Rev. B* **2012**, *86*, 115409. [[CrossRef](#)]
13. Peng, B.; Ang, P.K.; Loh, K.P. Two-Dimensional Dichalcogenides for Light-Harvesting Applications. *Nano Today* **2015**, *10*, 128–137. [[CrossRef](#)]
14. Fang, F.; Wan, Y.; Li, H.; Fang, S.; Huang, F.; Zhou, B.; Jiang, K.; Tung, V.; Li, L.-J.; Shi, Y. Two-Dimensional Cs₂AgBiBr₆/WS₂ Heterostructure-Based Photodetector with Boosted Detectivity via Interfacial Engineering. *ACS Nano* **2022**, *16*, 3985–3993. [[CrossRef](#)]
15. Huang, J.-K.; Pu, J.; Hsu, C.-L.; Chiu, M.-H.; Juang, Z.-Y.; Chang, Y.-H.; Chang, W.-H.; Iwasa, Y.; Takenobu, T.; Li, L.-J. Large-Area Synthesis of Highly Crystalline WSe₂ Monolayers and Device Applications. *ACS Nano* **2014**, *8*, 923–930. [[CrossRef](#)]

16. Liu, W.; Kang, J.; Sarkar, D.; Khatami, Y.; Jena, D.; Banerjee, K. Role of Metal Contacts in Designing High-Performance Monolayer n-Type WSe₂ Field Effect Transistors. *Nano Lett.* **2013**, *13*, 1983–1990. [[CrossRef](#)]
17. Luo, P.; Wang, F.; Qu, J.; Liu, K.; Hu, X.; Liu, K.; Zhai, T. Self-Driven WSe₂/Bi₂O₃Se Van Der Waals Heterostructure Photodetectors with High Light On/Off Ratio and Fast Response. *Adv. Funct. Mater.* **2021**, *31*, 2008351. [[CrossRef](#)]
18. Yu, X.; Prévot, M.S.; Guijarro, N.; Sivula, K. Self-Assembled 2D WSe₂ Thin Films for Photoelectrochemical Hydrogen Production. *Nat. Commun.* **2015**, *6*, 7596. [[CrossRef](#)]
19. Yu, X.; Guijarro, N.; Johnson, M.; Sivula, K. Defect Mitigation of Solution-Processed 2D WSe₂ Nanoflakes for Solar-to-Hydrogen Conversion. *Nano Lett.* **2018**, *18*, 215–222. [[CrossRef](#)]
20. Xia, J.; Liang, C.; Gu, H.; Mei, S.; Cai, Y.; Xing, G. Two-Dimensional Heterostructure of MoS₂/BA₂PbI₄ 2D Ruddlesden–Popper Perovskite with an S Scheme Alignment for Solar Cells: A First-Principles Study. *ACS Appl. Electron. Mater.* **2022**, *4*, 1939–1948. [[CrossRef](#)]
21. Hohenberg, P.; Kohn, W. Inhomogeneous Electron Gas. *Phys. Rev.* **1964**, *136*, B864–B871. [[CrossRef](#)]
22. Kohn, W.; Sham, L.J. Self-Consistent Equations Including Exchange and Correlation Effects. *Phys. Rev.* **1965**, *140*, A1133–A1138. [[CrossRef](#)]
23. Kresse, G.; Furthmüller, J. Efficiency of Ab-Initio Total Energy Calculations for Metals and Semiconductors Using a Plane-Wave Basis Set. *Comput. Mater. Sci.* **1996**, *6*, 15–50. [[CrossRef](#)]
24. Kresse, G.; Furthmüller, J. Efficient Iterative Schemes for Ab Initio Total-Energy Calculations Using a Plane-Wave Basis Set. *Phys. Rev. B* **1996**, *54*, 11169–11186. [[CrossRef](#)] [[PubMed](#)]
25. Kresse, G.; Joubert, D. From ultrasoft pseudopotentials to the projector augmented-wave method. *Phys. Rev. B* **1999**, *59*, 1758–1775. [[CrossRef](#)]
26. Perdew, J.P.; Burke, K.; Ernzerhof, M. Generalized Gradient Approximation Made Simple. *Phys. Rev. Lett.* **1996**, *77*, 3865–3868. [[CrossRef](#)]
27. Ernzerhof, M.; Scuseria, G.E. Assessment of the Perdew–Burke–Ernzerhof exchange–correlation functional. *J. Chem. Phys.* **1999**, *110*, 5029–5036. [[CrossRef](#)]
28. Heyd, J.; Scuseria, G.E.; Ernzerhof, M. Hybrid functionals based on a screened Coulomb potential. *J. Chem. Phys.* **2003**, *118*, 8207–8215. [[CrossRef](#)]
29. Jain, A.; Ong, S.P.; Hautier, G.; Chen, W.; Richards, W.D.; Dacek, S.; Cholia, S.; Gunter, D.; Skinner, D.; Ceder, G.; et al. Commentary: The Materials Project: A materials genome approach to accelerating materials innovation. *APL Mater.* **2013**, *1*, 011002. [[CrossRef](#)]
30. Feng, L.; Li, N.; Yang, M.; Liu, Z. Effect of pressure on elastic, mechanical and electronic properties of WSe₂: A first-principles study. *Mater. Res. Bull.* **2014**, *50*, 503–508. [[CrossRef](#)]
31. Chen, Y.; Shi, T.; Liu, P.; Ma, X.; Shui, L.; Shang, C.; Chen, Z.; Wang, X.; Kempa, K.; Zhou, G. Insights into the mechanism of the enhanced visible-light photocatalytic activity of black phosphorus/BiVO₄ heterostructure: A first-principles study. *J. Mater. Chem. A* **2018**, *6*, 19167–19175. [[CrossRef](#)]
32. Wang, V.; Xu, N.; Liu, J.-C.; Tang, G.; Geng, W.-T. VASPKIT: A user-friendly interface facilitating high-throughput computing and analysis using VASP code. *Comput. Phys. Commun.* **2021**, *267*, 108033. [[CrossRef](#)]
33. Low, J.; Jiang, C.; Cheng, B.; Wageh, S.; Al-Ghamdi, A.A.; Yu, J. A review of direct Z-scheme photocatalysts. *Small Methods* **2017**, *1*, 1700080. [[CrossRef](#)]
34. Cai, Y.; Zhang, G.; Zhang, Y.-W. Electronic properties of phosphorene/graphene and phosphorene/hexagonal boron nitride heterostructures. *J. Phys. Chem. C* **2015**, *119*, 13929–13936. [[CrossRef](#)]

Disclaimer/Publisher’s Note: The statements, opinions and data contained in all publications are solely those of the individual author(s) and contributor(s) and not of MDPI and/or the editor(s). MDPI and/or the editor(s) disclaim responsibility for any injury to people or property resulting from any ideas, methods, instructions or products referred to in the content.